DOI: 10.61782/fa.2025.0694

FORUM ACUSTICUM
EURONOISE 2025

PREDICTION OF FLANKING SOUND TRANSMISSION ACROSS PERIODIC CROSS-LAMINATED TIMBER JUNCTIONS WITH AREA COUPLINGS

Stijn Moons [1,2*] **Reinhilde Lanoye**[2] **Edwin P.B. Reynders**[1]

[1] Department of Civil Engineering, KU Leuven, Kasteelpark Arenberg 40, 3001 Leuven, Belgium
[2] CDM Stravitec, Reutenbeek 9/11, 3090 Overijse, Belgium

ABSTRACT

Cross-laminated timber (CLT) has gained popularity as a lightweight, carbon-neutral material for load-bearing walls and floors. However, its poor acoustic performance poses a crucial challenge to its further adoption. A critical factor is flanking sound, where vibrational energy is transmitted between two walls across a common junction. Typically, this transmission is analyzed with models based on plate or shell theory, but their accuracy at high frequencies is limited the ratio of wavelength to wall thickness is not large. While full-scale finite element analysis is possible, its computational cost at high frequencies is prohibitive as very fine element meshes are required. In the current study, an approach is presented which exploits the spatial periodicity often exhibited by CLT junctions. This allows the use of Bloch-Floquet analysis of the junction itself and the connected walls, leading to diffuse transmission coefficients between all wave types in the junction. The junction is treated as an elastic solid as opposed to the conventional thin shell modelling which results in a line coupling. Statistical Energy Analysis (SEA) is employed to compute the vibration reduction indices of the junction from these coefficients. The prediction model is applied to rigidly connected CLT junctions.

Keywords: *cross-laminated timber, flanking sound transmission, statistical energy analysis, periodic finite element method.*

**Corresponding author*: *stijn.moons@kuleuven.be.*

1. INTRODUCTION

Cross-laminated timber (CLT) has gained popularity as an alternative to more carbon-intensive materials for load-bearing structures such as concrete. However, its further adoption is hindered by a generally poor acoustic performance. Especially structure-borne sound poses a problem due to the low weight and relatively high stiffness of CLT, with flanking sound transmission often dominating the overall sound transmission. In this transmission mechanism, vibration energy is exchanged between connected walls across their common junction. As a result, CLT junctions are often designed to mitigate flanking sound transmission with solutions such as resilient interlayers or pads between a wall and the floor beneath it. While these solutions are often effective, a better, deeper understanding of the vibration transmission is required to optimize their design. Computationally efficient prediction models are important tools in the further development of vibration reducing solutions and CLT junctions in general, because of the large variation in transmission paths.

In a recent publication [1], an analytical prediction model for continuous CLT junctions was presented within a Statistical Energy Analysis (SEA) framework [2]. The CLT walls are modelled as directly connected homogeneous thin plates [3, 4]. While the broadband predictions are quite accurate, thickness effects are absent in this model, leading to prediction deviations in the high-frequency range. Numerical modelling with volumetric finite elements allows to take high-frequency thickness effects into account as well as the layered nature of CLT panels. While full-scale modelling of a building junction

is possible, the computation time is a limiting factor, especially at high frequencies where fine element meshes are required. Exploiting the spatial periodicity of the CLT junctions, it is possible to model only a repeated unit cell deterministically with the finite element method and apply Bloch-Floquet analysis to each connected wall as well as to the junction itself. The resulting approach is often termed as the periodic finite element method (pFEM). In this article, a prediction model for the vibration reduction index K_{ij} of CLT junctions is presented where the connected walls and the junction itself are modelled with a pFEM approach. The vibrational energy transmission is analysed in a SEA framework. Section 2 describes the general principles behind the prediction model. The model is validated with experimental laboratory measurements on a rigid CLT X-junction in Section 3.

2. THEORETICAL FRAMEWORK OF THE PREDICTION MODEL

Fig. 1 contains a schematic representation of the type of system that is being considered. The junction is connected to a total of n walls via area couplings. The assembly is spatially periodic in the global x-direction and the corresponding unit cell length is denoted as l_x. Each wall j is also spatially periodic in its local y-direction, with corresponding unit cell width $l_{\mathrm{y},j}$. In what follows, displacements $\mathbf{u}_j$ are expressed in the local coordinate system of wall j, unless stated otherwise. The subscript j is omitted for notational simplicity wherever possible.

Free plane waves in the periodic structure adhere to the Bloch-Floquet theorem, such that the displacements $\mathbf{u}(\mathbf{x},\mathbf{n})$, expressed in the local coordinate system of a wall, in any cell with position $\mathbf{n} = (n_\mathrm{x}, n_\mathrm{y})$ relative to the reference cell of the wall satisfy

$$\mathbf{u}(\mathbf{x},\mathbf{n}) = \mathbf{u}(\mathbf{x})\,\mathrm{e}^{-\mathrm{i}\epsilon_\mathrm{x}-\mathrm{i}\epsilon_\mathrm{y}}, \qquad (1)$$

for coordinates $\mathbf{x} = (x, y)$ within the reference unit cell. The factors ϵ_x and ϵ_y are the phase constants corresponding to a given wave [5]. Unit cells of the walls and junction itself are modelled deterministically with volumetric finite elements, allowing to compute the unit cell stiffness and mass matrices $\mathbf{K}$ and $\mathbf{M}$ of each component.

Figures 2 and 3 illustrate the unit cell for a connected wall and the junction beam with interfaces between connected elements indicated in grey. The nodes and corresponding degrees of freedom in the finite element model of each wall can be distributed into separate groups related to their position within the unit cell: left bottom (LB), right bottom (RB), bottom (B), left (L), right (R), left top (LT), right top (RT), top (T) and internal (I). By imposing Bloch boundary conditions on the unit cell with phase constants in the local x- and y-direction on the degrees of freedom as in equation (1), the system can be reduced by matrix $\mathbf{R}$ with $\mathbf{u}_\mathrm{full} = \mathbf{R}\mathbf{u}_\mathrm{red}$ to a system with only degrees of freedom LB, B, L and I. For free wave propagation, the equations of motions of a wall lead to the

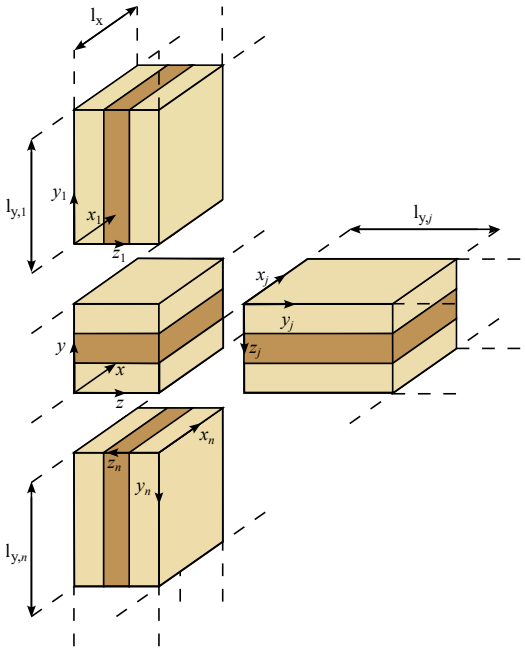

Figure 1. Exploded view of a T-junction with indication of the local coordinate systems of each element.

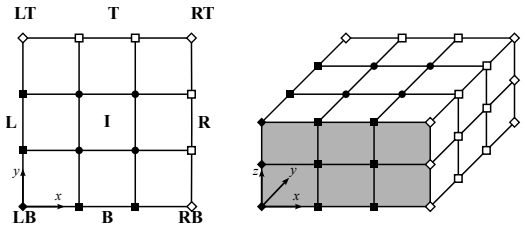

Figure 2. Unit cell of a wall with separate node labels.

following eigenvalue problem solved for eigenfrequencies ω and displacement eigenvectors $\boldsymbol{\phi}$, corresponding to the reduced degrees of freedom for displacements $\mathbf{u}_{\mathrm{red}}$:

$$\mathbf{R}^{\mathrm{H}}\left(\mathbf{K}-\omega^{2}\left(\epsilon_{\mathrm{x}},\epsilon_{\mathrm{y}}\right)\mathbf{M}\right)\mathbf{R}\boldsymbol{\phi}\left(\epsilon_{\mathrm{x}},\epsilon_{\mathrm{y}}\right)=0. \tag{2}$$

Similarly, the junction beam degrees of freedom are divided into: left (L), right (R), sleeve (S), left sleeve (LS), right sleeve (RS) and internal (I), which can be reduced to LS, L, S and I for an imposed ϵ_{x}.

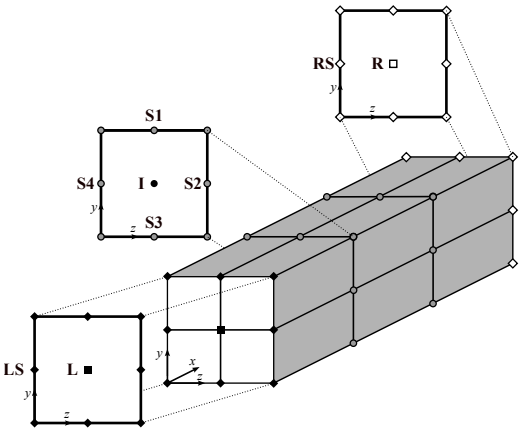

Figure 3. Unit cell of the junction beam with separate node labels.

The vibration transmission of the junction is analysed in a Statistical Energy Analysis (SEA) framework [2] with subsystems corresponding to free propagating wave types in a given connected element. In further derivations, the subscripts m and n are used to denote given source and receiver subsystems, respectively, such that a source subsystem m corresponds to wave type s in wall i and a receiver subsystem n to wave type t in wall j. The subsystems in all walls are assumed to be diffuse. Following a modal approach, this implies that each mode resonating within a given frequency band $\Delta\omega$, corresponding to a wave type with imposed phase constants ϵ_{x} and ϵ_{y}, has the same energy density e [6].

In order to study the energy exchange across the junction, the power balance of the overall SEA system is expressed in function of the subsystem energies E_m, input powers W_m, total loss factors η_m and coupling loss factors η_{mn} between subsystems m and n:

$$\begin{bmatrix}-\eta_1 & \eta_{21} & \eta_{31} & \dots\\ \eta_{12} & -\eta_2 & \eta_{32} & \dots\\ \eta_{13} & \eta_{23} & -\eta_3 & \dots\\ \dots & \dots & \dots & \dots\end{bmatrix}\begin{bmatrix}E_1\\E_2\\E_3\\\dots\end{bmatrix}=\begin{bmatrix}-W_1/\omega\\-W_2/\omega\\-W_3/\omega\\\dots\end{bmatrix}. \tag{3}$$

This system is solved for the subsystem energies E_m at each frequency of interest. The total number of subsystems and, therefore, the size of the SEA system may differ in function of frequency, as higher order wave types can cut on within the frequency range of interest. The system requires the computation of η_{mn}, η_m and W_m in function of frequency, where

$$\eta_m=\eta_{\mathrm{d},m}+\sum_{m=1}^{M}\eta_{mn}, \tag{4}$$

where $\eta_{\mathrm{d},m}$ is the equivalent internal loss factor of the subsystem. For laminates with layers with identical damping properties such as CLT, this value is equal to the material internal loss factor if edge radiation and damping are negligible.

The input power W_m per source subsystem m is derived in accordance with [7]; in the special case where the wall is excited on its top surface by a point load $\mathbf{F}$. This load is exerted in the z-direction at location $\mathbf{x}_0$ in a unit cell with position $\mathbf{n}_0$ relative to the reference unit cell. For a given surface traction $\mathbf{t}\left(\mathbf{x},\mathbf{n}\right)$, the resulting complex amplitude $a_m\left(\epsilon_{\mathrm{x}},\epsilon_{\mathrm{y}}\right)$ for a given subsystem is given by

$$a_m\left(\epsilon_{\mathrm{x}},\epsilon_{\mathrm{y}}\right)=\frac{\iint_A\boldsymbol{\phi}_m^{\mathrm{H}}\left(\mathbf{x},\mathbf{n}\right)\mathbf{t}\left(\mathbf{x},\mathbf{n}\right)\mathrm{d}X\mathrm{d}Y}{N_{\mathrm{x}}N_{\mathrm{y}}\left(\left(1+\mathrm{i}\eta_{\mathrm{d},m}\right)\omega_m^2-\omega^2\right)}, \tag{5}$$

where X and Y are the coordinates in the global coordinate system of the wall, which can also be indicated by $(\mathbf{x},\mathbf{n})$, A is the total surface area of the wall, N_{x} and N_{y} the number of unit cells in their respective dimensions and ω_m the eigenfrequency for subsystem m for an imposed phase constant combination. In the special case of an external point load, the traction corresponds to a spatial Dirac impulse with $\mathbf{t}=\mathbf{F}\delta\left(\mathbf{x}-\mathbf{x}_0\right)$ for an excitation location $(\mathbf{x}_0,\mathbf{n}_0)$. As a result, equation (6) can be simplified to

$$a_m\left(\epsilon_{\mathrm{x}},\epsilon_{\mathrm{y}}\right)=\frac{\boldsymbol{\phi}_m^{\mathrm{H}}\left(\mathbf{x}_0,\mathbf{n}_0\right)\mathbf{F}\left(\mathbf{x}_0,\mathbf{n}_0\right)}{N_{\mathrm{x}}N_{\mathrm{y}}\left(\left(1+\mathrm{i}\eta_{\mathrm{d},m}\right)\omega_m^2-\omega^2\right)}. \tag{6}$$

This amplitude is always a scalar and is computed for every source subsystem for the wave with phase constants

(ϵ_x, ϵ_y). The input power $W_m(\epsilon_x, \epsilon_y)$ for subsystem m for a point load excitation is given by

$$W_m(\epsilon_x, \epsilon_y) = \frac{1}{2}\mathrm{Re}\left\{\mathrm{i}\omega \mathbf{F}^{\mathrm{T}}(\mathbf{x}_0, \mathbf{n}_0)\, \mathbf{u}_m^*(\mathbf{x}_0, \mathbf{n}_0)\right\}, \quad (7)$$

where

$$\mathbf{u}_m(\mathbf{x}_0, \mathbf{n}_0) = a_m(\epsilon_x, \epsilon_y)\, \boldsymbol{\phi}_m(\mathbf{x}_0, \mathbf{n}_0). \quad (8)$$

The total subsystem input power per frequency band is obtained by summing the contribution of any (ϵ_x, ϵ_y) combination where its eigenfrequency ω_m lies within the frequency band of interest $\Delta\omega$. Born-Von Kárman (also termed periodic) boundary conditions are applied on the full wall to take the finite wall size into account, where the movement at opposite edges is continuous, such that the wave motion in the wall is spatially periodic. This enables the resonating modes in the wall to be composed of purely travelling waves in opposite directions. The range of imposed phase constants can be limited to the Brillouin zone of $[-\pi, \pi]$ [5]. For orthotropic structures such as CLT walls, this can be limited to $[0, \pi]$ due to symmetry.

The coupling loss factors η_{mn} between subsystems m and n are defined as

$$\eta_{mn} = \frac{W_{mn}}{\omega E_m}, \quad (9)$$

where W_{mn} is the power transmitted across the junction from m to n and $E_m = eV_iN_m$ with volume V_i of wall i and N_m the number of modes resonating in the frequency band of interest. The intensity in the local y-direction for a single resonating mode is $ec_{\mathrm{gy},m}$ with $c_{\mathrm{gy},m}$ the y-component of the group velocity. The transmitted power $W_{mn}(\epsilon_x, \epsilon_y)$ for imposed phase constants is given by

$$W_{mn}(\epsilon_x, \epsilon_y) = \tau_{mn}(\epsilon_x, \epsilon_y)\, S_{ij} e_m c_{\mathrm{gy},m}(\epsilon_x, \epsilon_y), \quad (10)$$

where S_{ij} is the area of the interface between the wall and the junction, and $\tau_{mn}(\epsilon_x, \epsilon_y)$ the transmission coefficient for an incident wave in subsystem m and transmitted or reflected wave to subsystem n. The total transmitted power W_{mn} in a frequency band is obtained by summing the contributions of each mode with resonance frequency within this frequency band, analogous to the input power.

The procedure to determine the transmission coefficients $\tau_{mn}(\epsilon_x, \epsilon_y)$ is a generalization of the approach of [3]. An incident wave of wave type s in source plate i with imposed phase constant ϵ_x and an arbitrary displacement amplitude impinges on the junction. Given that all system components exhibit the same spatial periodicity along the x-axis, all reflected and transmitted waves have the same phase constant. Additionally, the analysis is conducted at a frequency corresponding to the eigenfrequency of the incident wave. The interface forces of the unit cells of the different components, indicated in grey in Figures 2 and 3, should be in equilibrium, such that for the forces in global coordinates

$$\mathbf{f}_{\mathrm{jun}} + \mathbf{f}_{\mathrm{inc}} + \sum_{j=1}^{n} \mathbf{f}_j = \mathbf{0}, \quad (11)$$

where $\mathbf{f}_{\mathrm{jun}}$ represents the interface forces of the junction, $\mathbf{f}_{\mathrm{inc}}$ the interface forces of the incident wave in wall i, and $\mathbf{f}_j$ the interface forces of the outgoing waves in wall j. The forces in the walls for outgoing wave motion can be related to the interface displacements by exploiting the two-dimensional spatial periodicity. This leads to the dynamic stiffness matrix of wall j for outgoing wave motion, denoted as $\mathbf{D}_j(\epsilon_x, \omega)$. Furthermore, in the junction itself, the forces and displacements at the interface degrees of freedom can be coupled via a junction dynamic stiffness matrix $\mathbf{D}_{\mathrm{jun}}(\epsilon_x, \omega)$ by exploiting the one-dimensional spatial periodicity. As a result, one has that

$$\mathbf{D}_{\mathrm{jun}}\mathbf{u} + \mathbf{f}_{\mathrm{inc}} + \sum_{j, j\neq i} \mathbf{D}_j\mathbf{u} + \mathbf{D}_i(\mathbf{u} - \mathbf{u}_{\mathrm{inc}}) = \mathbf{0}, \quad (12)$$

where all displacements $\mathbf{u}$ are expressed in global coordinates. Note that $\mathbf{u}_{\mathrm{inc}}$ represents the displacements at the interface due to the incident wave motion only, which can be obtained by only considering one wavetype propagating in the $-y$-direction with fixed wave amplitude, so it is uniquely determined.

The procedure to derive the interface dynamic stiffness matrices $\mathbf{D}_j(\epsilon_x, \omega)$ follows that of [8]. The dynamic stiffness matrix of the unit cell $\mathbf{D} = \mathbf{K} - \omega^2\mathbf{M}$ is reduced to degrees of freedom LB and B by imposing ϵ_x, ω and solving ϵ_y from equation (2). This leads to an eigenvalue problem with $2N$ solutions in function of ϵ_y with eigenvectors composed of the modal displacements $\boldsymbol{\phi}_{\mathrm{u}}$ and forces $\boldsymbol{\phi}_{\mathrm{f}}$ at these degrees of freedom for all potential outgoing waves. The total interface displacements and forces $\mathbf{u}_j$ and $\mathbf{f}_j$ of wall j are computed from these eigen-

vectors as

$$\mathbf{u}_j = \sum_{n=1}^{N} a_n \boldsymbol{\phi}_{\mathrm{u}} = \mathbf{Q}\mathbf{a}, \tag{13}$$

$$\mathbf{f}_j = \sum_{n=1}^{N} a_n \boldsymbol{\phi}_{\mathrm{f}} = \mathbf{P}\mathbf{a}, \tag{14}$$

where $\mathbf{a}$ is a set of a priori unknown amplitudes. Given that $\mathbf{f}_j = \mathbf{D}_j \mathbf{u}_j$,

$$\mathbf{D}_j\left(\epsilon_{\mathrm{x}}, \omega\right) = \mathbf{P}\mathbf{Q}^{-1}. \tag{15}$$

Note that only N eigensolutions are taken into account, corresponding to outgoing waves propagating or decaying in the local $+y$-direction of the wall. For the junction beam, a similar procedure is followed to determine $\mathbf{D}_{\mathrm{jun}}$, exploiting the one-dimensional spatial periodicity along the x-axis. Solving equation (12) for the interface displacements $\mathbf{u}$ allows to determine the power related to each outgoing wavetype t in receiver wall j by decomposition of the wall edge displacements $\mathbf{u}_j$ within the full set of interface displacements $\mathbf{u}$ as in equations (13) and (14). The corresponding transmitted power per subsystem is given by

$$W_{mn}\left(\epsilon_{\mathrm{x}}, \epsilon_{\mathrm{y}}\right) := \frac{1}{2}\mathrm{Re}\left\{\mathbf{f}_{mn}^{\mathrm{T}} \mathbf{u}_{mn}^{*}\right\}. \tag{16}$$

The definition of incident wave power $W_{\mathrm{inc}}\left(\epsilon_{\mathrm{x}}, \epsilon_{\mathrm{y}}\right)$ is analogous. The transmission coefficients $\tau_{mn}\left(\epsilon_{\mathrm{x}}, \epsilon_{\mathrm{y}}\right)$ required in equation (10) are defined as

$$\tau_{mn}\left(\epsilon_{\mathrm{x}}, \epsilon_{\mathrm{y}}\right) := \frac{W_{mn}\left(\epsilon_{\mathrm{x}}, \epsilon_{\mathrm{y}}\right)}{W_{\mathrm{inc}}\left(\epsilon_{\mathrm{x}}, \epsilon_{\mathrm{y}}\right)}. \tag{17}$$

Finally, the measurement formula for the vibration reduction index K_{ij} between connected walls i and j following ISO 12354-1 [9] is given by

$$K_{ij} = \frac{\sum_{s,t} D_{\mathrm{vz},ij}^{st} + \sum_{s,t} D_{\mathrm{vz},ji}^{ts}}{2} + 10\log\frac{l_{ij}}{\sqrt{a_{\mathrm{eq},i} a_{\mathrm{eq},j}}}, \tag{18}$$

where l_{ij} is the junction length, $a_{\mathrm{eq},i}$ and $a_{\mathrm{eq},j}$ the equivalent absorption lengths of the walls and $D_{\mathrm{vz},ij}^{st}$ the transverse velocity level differences between the subsystems, defined as

$$D_{\mathrm{vz},ij}^{st} := 10\log\frac{< v_{mz}^2 >}{< v_{nz}^2 >} = 10\log\frac{E_{mz} m_j}{E_{nz} m_i}, \tag{19}$$

where $< v_{mz}^2 >$ denotes the surface-averaged squared velocity of subsystem m in the local z-direction, E_{mz} is the subsystem energy for the local z-components and m_i and m_j are the total masses of wall i and j, respectively. At resonance, the subsystem energy is given by

$$E_m = \frac{1}{4}\left|a_m\right|^2 \boldsymbol{\phi}_m^{\mathrm{H}} \left(\mathbf{K} + \omega_m^2 \mathbf{M}\right) \boldsymbol{\phi}_m, \tag{20}$$

for an amplitude a_m such that $\mathbf{u}_m = a_m \boldsymbol{\phi}_m$. Equation (3) is solved for the total band-averaged subsystem energies per subsystem E_m. The transverse subsystem energy E_{mz} can be computed by only taking the z-components of $\boldsymbol{\phi}_m$ into account. Both $E_{mz}\left(\epsilon_{\mathrm{x}}, \epsilon_{\mathrm{y}}\right)$ and $E_m\left(\epsilon_{\mathrm{x}}, \epsilon_{\mathrm{y}}\right)$ are calculated with equation (20) for each phase constant combination, after which their values are band-averaged in the same way as the input power. The subsystem energies resulting from equation (3) are then multiplied by the ratio E_{mz}/E_m per frequency band for each subsystem. In this way, all contributions to the transverse wave motion and therefore, the sound radiation, are taken into account in equation (18) for K_{ij}.

3. RESULTS AND DISCUSSION

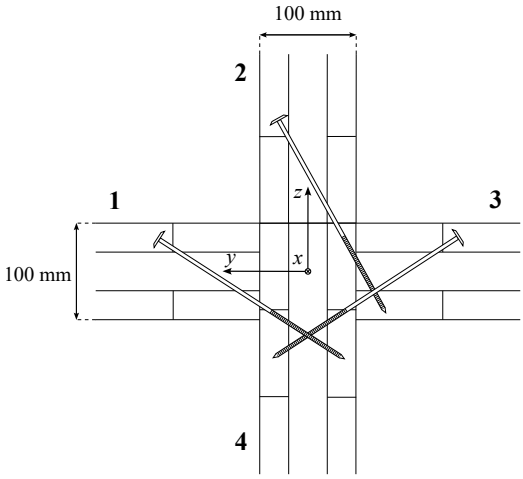

Figure 4. Configuration of the junction with screw positions.

The prediction model is validated with laboratory measurements of the vibration reduction index K_{ij} for a CLT X-junction consisting of 4 walls [11, 12]. Each wall is a 3-ply cross-laminated timber panel with a layer stacking of [0 π/2 0] relative to the global $x-$axis. The material properties of a single timber layer of strength class C24 are summarized in Table 1. Each layer has

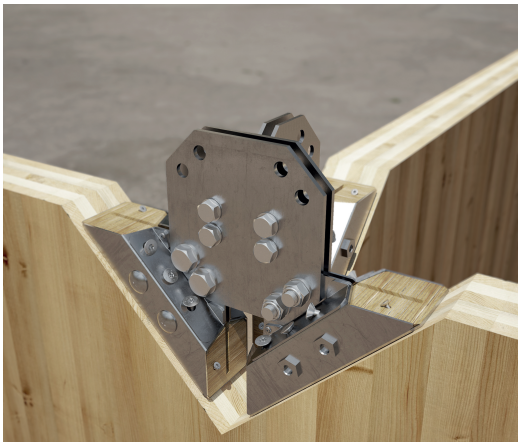

Figure 5. Rotationally stiff X-RAD connector [10].

Table 1. Mechanical properties of timber of strength class C24 [13].

ρ [kg/m^3]	E_x [MPa]	E_y [MPa]	G_xy [MPa]	ν_yx [-]
450	11 000	367	690	0.014

an assumed internal loss factor of 0.02. The structural wall connections are obtained either by screws or more rotationally stiff connectors, displayed in Figure 5. Figure 4 illustrates the junction configuration including the screw positions.

The vibration reduction indices are predicted with the pFEM model detailed in the previous section, where the panels are modelled with 8-node solid volume elements, with each timber layer modelled separately. Due to the homogeneity of the CLT in the lateral directions of each wall, the unit cell can be taken arbitrarily small to reduce computation time. The junction beam is also considered as a CLT volume with a lateral dimensions corresponding to the thicknesses of the connected walls. In this example, the screws or the other connector are not modelled explicitly, but in this prediction framework this is a future possibility. Additionally, predictions with an analytical wave approach model for thin homogeneous plates, directly connected along a massless line connection [1]. This requires the mechanical properties for an homogeneous plate equivalent to the CLT panel. They are determined with the modified gamma method [14], imposing static equivalence between the transverse bending stiffness of the separate layers and an equivalent single-layer

Table 2. Mechanical properties for an equivalent single-layer CLT panel.

ρ [kg/m^3]	E_x [MPa]	E_y [MPa]	G_xy [MPa]	ν_yx [-]
450	7 533	768	690	0.149

panel, summarized in Table 2. For both models, equivalent absorption lengths $a_{\mathrm{eq},j}$ were determined from the experimentally determined structural reverberation times $T_{\mathrm{s},j}$:

$$a_{\mathrm{eq},j} = \frac{2.2\pi^2 S_j}{T_{\mathrm{s},j} c_0 \sqrt{f/f_\mathrm{ref}}}, \tag{21}$$

where $c_0 = 343\,\mathrm{m/s}$, $f_\mathrm{ref} = 1000\,\mathrm{Hz}$ and S_j the surface area of wall j. As another reference for comparison, the empirical K_{ij} formulae from Annex F of ISO 12354-1 [9] for rigid CLT junctions were applied for the transmission paths as follows

$$K_{12} = 18.8 + 3.3\log\left(\frac{f}{f_\mathrm{k}}\right), \tag{22}$$

$$K_{13} = 23 + 3.3\log\left(\frac{f}{f_\mathrm{k}}\right), \tag{23}$$

$$K_{24} = 10 - 3.3\log\left(\frac{f}{f_\mathrm{k}}\right) + 10M, \tag{24}$$

where $f_\mathrm{k} = 500\,\mathrm{Hz}$ and $M = \log\left(m"_{\perp,j}/m"_j\right)$ for surface masses $m"_j$ and $m"_{\perp,j}$ for wall j and the wall perpendicular to it. Figures 6 up to 7 display the predicted values alongside the measured values for the corner transmission paths, the coplanar transmission path and the continuous coplanar transmission path. Prediction results are illustrated by black lines; coloured lines indicate experimental values, with red lines for the rotationally stiff connector in Figure 5 and blue lines for the screwed junction in Figure 4.

While the global frequency trend established by the empirical formulae from the international standard is more or less correct with the exception of path $2-4$, they are a clear oversimplification of the actual K_{ij} as the material and geometric parameters and connection type are not taken into account, leading to deviations of over 5 dB in most 1/3 octave bands.

Both prediction models showcase a correct frequency trend with generally closer correspondence to K_{ij} for either experimental configuration than the empirical formulae. As noted in [1], the analytical prediction model typ-

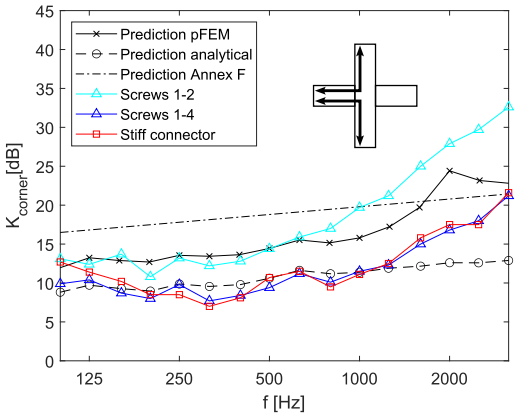

Figure 6. Vibration reduction index for the corner transmission paths in the CLT X-junction.

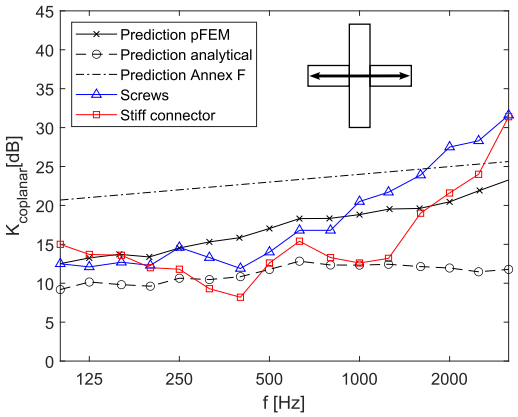

Figure 7. Vibration reduction index for the interrupted coplanar transmission path in the CLT X-junction.

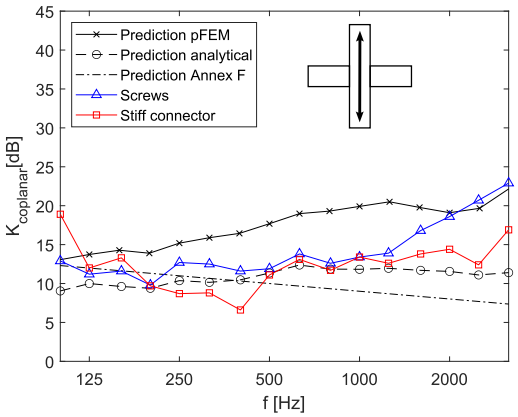

Figure 8. Vibration reduction index for the uninterrupted coplanar transmission path in the CLT X-junction.

ically offers a lower limit for K_{ij} due to the assumption of a rotationally stiff line connection. Therefore, it corresponds most closely to the results for stiffer connection types such as the X-RAD and the screwed junction for transmission path 1-4 which, unlike path 1-2, has a direct screw connection. Notably, the predictions are less accurate in the high-frequency range, where the thin plate assumption is typically invalid due to the small wavelengths compared to the wall thickness. As a result, the high-frequency K_{ij} increase is underestimated for each transmission path. Due to the inclusion of thickness effects, the new pFEM prediction model performs better in the high-frequency range. In general, the predicted K_{ij} values are several dB higher than the analytical model. One potential reason for this is the layered finite element modelling of the CLT walls, while homogenized single-layer values are used for the thin plate model which are not necessarily fully equivalent. Additionally, the junction itself has a mass and volume unlike the line connection in the analytical model, which could lead to a globally less stiff connection. While the thin plate model corresponds more closely to the stiffly connected transmission paths such as corner path 1-4 for the screws, the opposite holds for the pFEM model with the exception of the high-frequency range. Most notably, K_{24} across continuous coplanar transmission path 2-4 is better represented by the thin plate model, although the pFEM predictions are still relatively accurate. Note that the pFEM prediction results can be improved by explicitly including the screws

or X-RAD connector in the finite element model. Similarly, it is possible to implement flexible connectors (e.g. resilient pads) in future work, which allows for much design freedom and detail when modelling various building junctions. In general, the difference between the pFEM K_{ij} predictions and the experimental values lie beneath 5 dB for most 1/3 octave bands, with especially good correspondence to K_{ij} for connections with lower rotational stiffness. For example, the pFEM predictions of K_{12} differ less than 2 dB from the experimental results for the screw connection up to 1000 Hz.

4. CONCLUSIONS

The presented work introduces a prediction model for the vibration reduction index K_{ij} across CLT junctions with spatial periodicity along the junction direction, constructing finite element models for a repeated unit cell and applying Bloch analysis. The prediction model is validated with rigid X-junctions consisting of 3-ply CLT walls, connected by screws or more rotationally stiff modular connectors. The predicted values are quite accurate with differences with experimental results beneath 5 dB in most 1/3 octave bands and even lower for less rigid connections. Due to the large modelling freedom in this framework, it is possible to further improve the predictions by including resilient or stiff elements (e.g. resilient pads and screws, respectively) in future work.

5. ACKNOWLEDGMENTS

The research was funded by a Baekeland fellowship (HBC.2022.0712) from Flanders Innovation & Entrepreneurship (VLAIO).

6. REFERENCES

[1] S. Moons, R. Lanoye, and E. Reynders, "Prediction of flanking sound transmission through cross-laminated timber junctions with resilient interlayers," *Applied Acoustics*, vol. 228, January 2025.

[2] R. Craik, *Sound transmission through buildings using statistical energy analysis*. Aldershot, UK: Gower, 1996.

[3] R. Langley and K. Heron, "Elastic wave transmission through plate/beam junctions," *Journal of Sound and Vibration*, vol. 143, no. 2, pp. 241–253, 1990.

[4] I. Bosmans, P. Mees, and G. Vermeir, "Structure-borne sound transmission between thin orthotropic plates: analytical solutions," *Journal of Sound and Vibration*, vol. 191, pp. 75–90, May 1996.

[5] L. Brillouin, *Wave propagation in periodic structures*. New York City, NY,: Dover Publications, 2 ed., 1953.

[6] R. Lyon, "Needed: a new definition of diffusion," *Journal of the Acoustical Society of America*, vol. 56, pp. 1300–1302, October 1974.

[7] V. Cotoni, R. Langley, and P. Shorter, "A statistical energy analysis subsystem formulation using finite element and periodic structure theory," *Journal of Sound and Vibration*, vol. 318, pp. 1077–1108, 2008.

[8] R. Langley and V. Cotoni, "The direct field boundary impedance of two-dimensional periodic structures with application to high frequency vibration prediction," *The Journal of the Acoustical Society of America*, vol. 127, pp. 2118–2128, 2010.

[9] International Organization for Standardization, *Building acoustics — Estimation of acoustic performance of buildings from the performance of elements — Part 1: Airborne sound insulation between rooms*. Geneva, Switzerland, 2017.

[10] Rothoblaas, "X-RAD:X-RAD connection system." `https://www.rothoblaas.com/products/fastening/brackets-and-plates/x-rad/x-rad`.

[11] "Flanksound project," tech. rep., Rothoblaas, Bolzano, Italy, November 2016.

[12] F. Morandi, S. De Cesaris, M. Garai, and L. Barbaresi, "Measurement of flanking transmission for the characterisation and classification of cross laminated timber junctions," *Applied Acoustics*, vol. 141, pp. 213–222, July 2018.

[13] Austrian Institute of Construction Engineering, "European technical assessment eta-14/0349," Technical assessment ETA-14/0349, Austrian Institute of Construction Engineering, Vienna, Austria, 2020.

[14] J. Zhou, Y. Hei Chui, M. Gong, and L. Hu, "Elastic properties of full-size mass timber panels: Characterization using modal testing and comparison with model predictions," *Composites Part B: Engineering*, vol. 112, pp. 203–212, March 2017.